Journal of Materials Chemistry B

Accepted Manuscript

ROYAL SOCIETY OF CHEMISTRY

www.rsc.org/materialsB

One-step synthesis of water-dispersible silicon nanoparticles and their use in Fluorescence Lifetime Imaging of living cells

Jing Wang, Dai-Xin Ye, Guo-Hai Liang, Jian Chang, Ji-Lie Kong, Ji-Yao Chen**

J. Wang, J. Chang, Prof. J.Y. Chen
State Key Laboratory of Surface Physics and Department of Physics, and Key Laboratory of Micro and Nano Photonic Structures (Ministry of Education)
Fudan University
Shanghai 200433, People's Republic of China
**E-mail: jychen@fudan.edu.cn; Fax: +86-21-65104949; Tel.: +86-21-65643084.*

D. Ye, G. Liang, Prof. J.L. Kong
Department of Chemistry and Institutes of Biomedical Sciences, Fudan University, Shanghai, 200433, China
E-mail: jlkong@fudan.edu.cn; Fax: (+)86-21-65641740

Keywords: silicon nanoparticles; auto-fluorescence, time-correlated single photon counting; fluorescence lifetime Imaging.

We report a novel method of synthesizing water-dispersible silicon nanoparticles (Si NPs) with a simple one-step procedure using the mild reagents (3-aminopropyl) trimethoxysilane (APTES) and ascorbate sodium (AS). This is the first report of "green" synthesis of Si NPs on a large scale and at low cost. The method consists of a quick reaction in a commonly used round bottom flask at room temperature and pressure without additional treatment and any special equipment. The as-prepared Si NPs have an average diameter of 2 nm and emission band at 530 nm with a full width at half maximum height (FWHM) of 70 nm and quantum yield (QY) of 0.21. Moreover, the fluorescence lifetime of these Si NPs is much longer than that of native fluorophores in living cells. Therefore, these Si NPs allow effective imaging of living cells with a fluorescence lifetime imaging microscope (FLIM). Using the time gating model in FLIM, an excellent image was obtained in which the auto-fluorescence interference of

cellular fluorophores was suppressed demonstrating that the Si NPs are promising probes for cell imaging particularly with the FLIM technique.

#The first two authors give equal contribution to this work.

Introduction

As a new generation fluorescence probe, the semiconductor quantum dot (QD) has been widely used in bio-medical imaging and detection.[1-5] However, the commonly used QDs are cadmium based and their toxicity is still a problem in biological applications.[6,7] Silicon (Si) is a well-studied material in the semiconductor family, which is inert, abundant, economical and nontoxic. These advantages have promoted the development of Si NPs for bio-medical applications, as Si NPs also exhibit effective visible emission due to 1) the suitable surface modification favoring the radiative recombination and 2) the quantum confinement effect.[8-12] In the preparation of fluorescent Si NPs, the surface modification is most important factor. So far different methods of synthesis have been reported including ultrasonic dispersion of electrochemically etched silicon,[13] laser-driven pyrolysis of silane,[14,15] gas phase synthesis,[16] microemulsion synthesis,[17] synthesis in supercritical fluids,[12,18] and wet chemistry techniques such as —reduction of Zintl salts in inert organic solvents[19,20] and in micelles by sodium, hydride reagents.[21,22] However, Si NPs made by above methods are all hydrophobic, thus far, studies of water-dispersible Si NPs for biological applications are limited. Li et al grafted the polyacrylic acid (PAAc) on the surface of Si NPs to prepare water-soluble Si NPs and stained living cells with

these fluorescent Si PNs for the first time.[23] Sato et al reported water-dispersible Si NPs with propionic acid (PA) coating.[24] However, PAAc and PA coatings on Si NPs should be under UV irradiation for a long time. Warner et al synthesized allylamine capped Si NPs at room temperature through multistep reactions with hydride reducing agents.[25] Li et al further developed diphenylamine (DI) and carbazole (CA) capped Si NPs with a fluorescence quantum yield (QY) up to 0.75,[26] but the toxicity of DI and CA may limit their bio-medical applications.[27,28] Recently, Zhong et al developed a one-pot aqueous synthesis method for preparing Si NPs with the help of microwave irradiation because the reduction reagent trisodium citrate needs a reaction temperature of 160°C.[29] Although this work has promoted the progress of Si NPs as the fluorescent probes, finding a simple method to synthesize Si NPs at room temperature and pressure that eliminates high-temperature processing, special conditions and equipment, and tedious procedures is still a challenge.

Here, we used the mild reagents (3-aminopropyl) trimethoxysilane (APTES) and ascorbate sodium (AS) to achieve one-step facile synthesis of water-dispersible Si NPs at room temperature and pressure. In contrast to Zhong's synthetic route using $C_6H_{17}NO_3Si$ as the silicon source and trisodium citrate ($C_6H_5Na_3O_7$) as reduction reagent,[29] herein the APTES and As were used as the Si source and the reduction reagent to prepare the Si NPs. Since the AS has higher reduction property than trisodium citrate, one-step facile synthesis of water-dispersible Si NPs can be prepared at room temperature and pressure. The whole reaction process requires a common round bottom flask, without any special equipment, fulfilling the "green"

synthesis. The resulting Si NPs have a small size of 2 nm and are water-dispersible, highly fluorescent (QY: 21%), well biocompatible, strongly photo- and pH-stable, and superbly suitable for long-term cell imaging. Moreover, we demonstrate for the first time that the resulting Si NPs can act as promising fluorescence probes for time-resolved imaging of living cells greatly overcoming cellular auto-fluorescence background. The result shows that the combination of Si NPs with fluorescence life-time imaging microscope (FLIM) is a powerful approach for cell imaging.

RESULTS AND DISCUSSION

Si NPs was synthesized simply by facile mixing and stirring the reagents APTES and AS under room temperature for 30 min. By using this "green" method, we can obtain 0.1 g Si NPs in a single batch, as shown in **scheme 1**.

Transmission electron microscopy (TEM) image of Si NPs is shown in **Figure 1**A, in which the Si NPs appear as spherical particles. The inset of **Figure 1**A gives the size distribution of Si NPs with the average diameter of 1.8±0.4 nm, calculated by measuring more than 100 particles in TEM images. High-resolution TEM (HRTEM) image (**Figure 1** B) reveals the high crystallinity of the Si NPs. The lattice spacing of 0.31 nm agrees with diamond lattice of Si (111). Elemental analysis of the sample using energy-dispersive X-ray spectroscopy (EDS) is shown in Figure 1C. The analysis clearly indicates the presence of silicon, carbon and copper in Si NPs. The structures of the Si NPs were further characterized by atom force microscopy (AFM, **Figure 1** D and E). The AFM measurements suggest that the Si NPs have an average size of about 2 nm in diameter. The optical absorption and fluorescence spectra of the

Si NPs are shown in **Figure 1**F. The gradual increase in absorbance with a decrease in the wavelength from the onset wavelength of 450 nm, corresponding to the absorption edge of 2.75 eV, is a characteristic of absorption across the indirect band gap.[24] The emission spectrum of Si NPs in aqueous solution is centered at 530 nm with a full width at half maximum height (FWHM) of 70 nm (430 nm excitation). The emission QY was determined to be 21%. The aqueous solution of Si NPs exhibits intense green fluorescence under UV irradiation which is strong enough to be seen with the naked eye. To examine the main chemical bonds of Si NPs, FTIR spectrum was obtained (**Figure 1**G). The sharp absorbance peak at ~1200 cm^{-1} was ascribed to the vibrational stretch of Si−O bonding. The absorbance in the range of 2870 – 2960 cm^{-1} was attributed to the deformation and stretch vibration of the O-H bond. The strong absorbance at 1590 and 3400 cm^{-1} were assigned to N−H bending vibration and N−H stretching vibration, respectively. The present of $-NH_2$ terminal group make the Si NPs positively charged. The zeta potential of ~ +30 mV confirmed that these Si NPs have the positive charges on surfaces (**Figure 1**H). The surface positive charges make particles repel each other and well dispersed in aqueous solution. The positively charged surfaces also offer great advantages for cell staining, as the surface of living cells is negatively charged. The diameters of Si NPs in aqueous solution measured by dynamic light scattering (DLS) confirm again the small size of the Si NPs with a hydrodynamic diameter of 2.8 nm in **Figure 1**I. The hydrodynamic diameter of particles measured in solution by DLS is usually bigger than their solid diameter measured by TEM.[30,31] Importantly, the small size offers the advantage of particles for

biomedical applications, since particles with a diameter <5 nm benefit the renal clearance in vivo.[32]

The water-solubility and high-emission QY properties make Si NPs suitable as fluorescence probes for cell labeling. However, to get the effective emission of Si NPs the excitation wavelength should be shorter than 450 nm (see **Figure 1**F). **Figure 2** shows the confocal images of KB cells stained with Si NPs (B) and the control KB cells without any probe staining (A), under the excitation of a 405 nm laser and acquired by a PMT with a band-pass filter of 505-550 nm. Bright green fluorescence (left column) of the **Figure 2**B can be clearly seen in the Si NPs loaded cells. These cells have been incubated with 50 μg/ml Si NPs for 1.5 h. However, as shown in **Figure 2**A the auto-fluorescence of native fluorophores in control KB cells was also observed. Therefore, the green fluorescence image in **Figure 2**B should be the sum of the fluorescence of cellular Si NPs and auto-fluorescence of native fluorophores. After quantitatively measuring the fluorescence intensities in **Figure 2**A and 2B, the fluorescence image of **Figure 2**B is estimated to contain about 18% contribution of auto-fluorescence, which certainly induces an artificial effect in the imaging measurements of cellular Si NPs. There are a lot of native fluorophores, such as NADH and flavins, in living cells, and these fluorophores exist in any living system. The wavelengths in the region of 400-450 nm particularly favor the excitation of NADH and flavins producing a strong auto-fluorescence in the wavelength region of 450-550 nm.[33] In common fluorescence intensity imaging measurements for the living targets, the interference of auto-fluorescence seems unavoidable and also occurred

here in the measurement of cellular Si NPs.

To overcome the interference of the auto-fluorescence of native fluorophores, the characteristic of long emission lifetime of Si NPs can be utilized. The fluorescence lifetime of these cellular fluorophores is shorter than 5 ns.[34] The fluorescence image of cellular Si NPs was expected to be distinguished from the auto-fluorescence of native fluorophores by FILM, thus greatly eliminate the interference of the auto-fluorescence.

The fluorescence decay of Si NPs as well as the commonly used fluorescence probes FITC and rhodamine B were measured with time-correlated single photon counting (TCSPC) under the excitation of a pico-second (ps) 405 nm laser pulse. As shown in **Figure 3**, the fluorescence lifetime of Si NPs is obviously longer than that of FITC and rhodamine B. These decay curves can be fitted by exponential functions. To fit the decay traces of Si NPs, three exponential functions with acceptable residuals ($0.9 < \chi^2 < 1.1$) were required as shown in the following formula. The average fluorescence lifetime can then be obtained accordingly (see Experimental Section).

$$I(t) = \alpha_1 e^{(-t/\tau_1)} + \alpha_2 e^{(-t/\tau_2)} + \alpha_3 e^{(-t/\tau_3)}$$

Where I(t) is the measured fluorescence intensity as a function of time, t, after the excitation pulse. The calculated average lifetime (τ) of the Si NPs is 10.2 ns whereas the average lifetimes of rhodamine B and FITC are 2.2 ns and 2.4 ns.

When cells have been treated with Si NPs or FITC, the FLIM images of control cells, FITC stained cells and Si NPs incubated cells were measured, respectively

(**Figure 4**). The upper row of **Figure 4** shows the integrated fluorescence intensity images (1.2-13.2 ns). The autofluorescence image of control cells is shown in **Figure 4**A_1, so that the images of both FITC and Si NP-labeled cells (**Figure 4**B_1 and $4C_1$) contain the auto-fluorescence distribution of native cellular fluorophores. The lower row of **Figure 4** shows FLIM images with the color-marked fluorescence lifetime characteristic from 1.2 ns (red) to 13.2 ns (blue) (see the lifetime color bar in the right side of the main figure). The orange color in control cells (**Figure 4**A_2) confirms that the lifetime of auto-fluorescence is approximately 2 ns. The FITC-stained cells also exhibit the orange color with a stronger intensity compare to control cells, because the lifetime of FITC is 2.4 ns (**Figure 3**). The green-blue colors of Si NPs stained cells reflect the long fluorescence lifetime of cellular Si NPs (10-12 ns), which can be easily distinguished from the orange auto-fluorescence. Therefore, with the long fluorescence lifetime characteristic the Si NPs are suitable fluorescence probes for cell imaging with FLIM.

With the time-gating model of FLIM, the good quality of FLIM images can be further demonstrated. Because the fluorescence lifetimes of native fluorophores are shorter than 5 ns and those of Si NPs longer than 5 ns, two gating periods of 1-5 ns and 5-12 ns were settled to show the time-gating intensities of FLIM images of control cells, FITC- stained cells and Si NP-loaded cells. The upper row of **Figure 5** are time-gating intensity images acquired in 1-5 ns time period, whereas the low row shows the time-gating intensity images recorded in the 5-12 ns period after the excitation of the laser pulse. The time-gating images of control cells and FITC-stained

cells are clearly shown in the upper row (1-5 ns) but disappeared in most imaging region in the low row (5-12 ns), reflecting that the auto-fluorescence of native fluorophores would not interfere the measurement in the low row with the gating time of 5-12 ns. The good quality image of cellular Si NPs in Si NP-loaded cells is clearly seen in the low row (5-12 ns) and the image in upper row (1-5 ns) is the auto-fluorescence image of these Si NP-loaded cells. Using the time-gating technique of FLIM, the image of cellular Si NPs can be easily distinguished from the auto-fluorescence image of native fluorophores, and thus the excellent image of Si NP-loaded cells was obtained.

For measurements of fluorescence probes in living systems, the interference from the auto-fluorescence of native fluorophores is a tough problem. In particular, these native fluorophores such as NADH are very important molecules in living organisms. Increasing the fluorescence QY of the probe has been attempted as a method of decreasing the interference effect of auto-fluorescence. However, in some living systems the native fluorophore contents is high, so that the interference of auto-fluorescence is still serious even the high QY probe is used. The fluorescence lifetimes of these native fluorophores are less than 5 ns; thus the usage of the long fluorescence lifetime probes combined with the FLIM is a feasible method to overcome the interference of auto-fluorescence. Unfortunately, the fluorescence lifetimes of commonly used probes such as FITC and rhodamine, are all equally short (2-3 ns) as that of native fluorophores; therefore, these probes have no potential in FLIM applications. As demonstrated in **Figures 4** and **5**, Si NPs can be excellent

probes for cell imaging with FLIM overwhelmingly eliminating the auto-fluorescence interference of cellular fluorophores.

As fluorescence probes, the photostability of the probes is another important issue. **Figure 6**A and 6E show the fluorescence images of FITC and Si NPs labeled KB cells, respectively. With the continuous scanning model and the same excitation power of 488 nm laser for FITC and 405 nm laser for Si NPs, the fluorescence images of cellular FITC and Si NPs with scanning time were acquired, respectively, and shown in **Figure 6**. The photostability of FITC is poor as the FITC fluorescence has been photobleached after 3 minutes laser scanning. In contrast, the photostability of Si-NPs in cells is quite good. The fluorescence image of cellular Si-NPs almost has no decrement after 30 minutes laser scanning (**Figure 6**H), demonstrating that the Si-NPs are well qualified as the stable fluorescence probes particularly for long-term cell imaging.

For probes used in living systems, toxicity is a great concern. The cytotoxicity of Si NPs was evaluated by the 3-(4,5-dimethylthia-zol-2-yl)-2, 5-diphenyltetrazolium bromide (MTT) assay. The cell viabilities of KB cells incubated with different concentrations of Si NPs for 24 h were measured. As shown in **Figure 7**A, the cytotoxicity of Si NPs is very low. When the incubation concentration of Si NPs increases to 200 μg/ml, the slight damage just begins. Noting that the incubation time of Si NPs in this toxicity experiment was 24 h and the incubation time of Si NPs in cell staining experiments was only 1.5 h, the cytotoxicity of Si NPs can be neglected. **Figure 7**B shows the emission stability of Si NPs at varying pH. In the wide pH range

of 3−11, the fluorescence emission of Si NPs is very stable, reflecting that the Si NPs fit the requirement of qualified probes. Their stability and safety support Si NPs as suitable probes in bio-medical applications.

Conclusions

In summary, Si NPs were prepared by a simple one-step synthesis at room temperature and pressure. The positively charged surface allowed Si NPs to easily penetrate into living cells for staining and imaging purposes. The long fluorescence lifetime of Si NPs is particularly useful in cell imaging with FLIM, overwhelmingly suppressing the auto-fluorescence interference of cellular fluorophores which is a tough problem in common fluorescence intensity imaging measurements. Combine with the other advantages such as pH stability, photostability and safety to biological systems, Si NPs exhibit promise as excellent fluorescence probes in bio-medical applications.

Experimental Section

Preparation of Si NPs. APTES (97%) and AS were purchased from Sigma-Aldrich. The Si NPs were prepared by adding 1 mL of APTES to 4 mL aqueous solution while stirring. Then, 1.25 mL 0.1 M of AS was added to the above mixture stirring for 20 min. The total synthesis was completed in 30 min. The resulting Si NPs sample exhibited an intense green fluorescence under UV irradiation. By adjusting the ratio of APTES and AS and reaction time, the size of Si NPs can be controlled. The size of the Si NPs was determined by a TEM machine at 200 kV (JEOL JEM-2010F). The morphologies of the Si NPs were investigated by AFM

(Solver P47-MDT) in contact mode in air. Fluorescence spectra were recorded by a Horiba JobinYvon fluoromax-4 spectrofluorometer equipped with a HORIB-F-3004 sample heater/cooler (Peltierthermocouple drive) and F-3018 quantum yield accessory software. The absorption spectra were measured by spectrophotometer (Hitachi U-500). Fourier transform infrared (FT-IR) spectra were obtained using an IRPRESTIGE-21spectroscope (Shimadzu) with KBr pellets. Light-scattering analysis was performed to measure the hydrodynamic diameter of Si NPs in aqueous solution using a DynaPro dynamic light scattering (DLS), which was made by Malvern Corp, U.K. (ZEN3690). The zeta potentials of the Si NPs were measured in water solutions using a Malvern Zetasizer (ZEN 3600, Worcestershire, UK).

Cell Culture and Cell Treatments with Si NPs. The human nasopharyngeal carcinoma cells (KB) were obtained from the cell bank of Shanghai Science Academy. The cells were seeded in culture dishes containing DMEM medium with 10% calf serum, 100 units mL^{-1} penicillin, 100 μgmL^{-1} streptomycin and 100 μgmL^{-1} neomycin, and incubated in a fully humidified incubator at 37°C with 5% CO_2. When the cells reached 80% confluence with normal morphology, these cells were ready for further experiments.

Cell imaging experiments. A 50 μg/mL Si NPs or 3 μg/mL FITC in serum-free medium was added to the culture dish. After incubation at 37°C in a 5% CO_2 atmosphere for 1.5 h, cells were washed three times with phosphate buffered solution (PBS) to remove unbound compounds and were added with the fresh culture medium. The cell samples were then ready for imaging measurements. The fluorescence

images of cellular Si NPs were acquired with a laser scanning confocal microscope (LSCM) (Olympus FV300, IX71) in detection channel 2 with a 505-550 nm band-pass filter. Differential interference contrast (DIC) images were recorded simultaneously in a transmission channel to examine cell morphology. A water immersion objective (UplanApo, 60X, 1.2 NA) and a matched pinhole were used in experiments. A 405 nm laser (Coherent, Radius 405-25) was introduced into the LSCM for excitation.

Fluorescence lifetime measurements by TCSPC. Time-correlated single photon counting (TCSPC) is based on the detection of single photons of a periodic light signal and the reconstruction of the waveform from the time measurements. A 2×10^7 Hz 405nm pico-second (ps) laser (Edinburgh Instruments, EPL405) was used to excite the fluorescence probes in aqueous solution. The fluorescence decay courses of Si NPs and the organic dyes were measured using a PMT (Hamamatsu, R928P) with a band-pass filter of 520±20 nm in the TCSPC (Edinburgh Instruments, TCC900). The obtained fluorescence decay curves can be fitted with multi-exponential decay as described in Eq (1).

$$I(t) = \sum_{i=1}^{n} \alpha_i \exp\left(-\frac{t}{\tau_i}\right) \quad (1)$$

where τ_i and α_i represent the decay constant and amplitude of each exponential component, respectively. The average lifetime τ can be obtained according to the Eq (2).[35]

$$\bar{\tau} = \frac{\sum_{i=1}^{n} \alpha_i \tau_i^2}{\sum_{i=1}^{n} \alpha_i \tau_i} \quad (2)$$

With the numerous measurements, the average fluorescence lifetimes of Si NPs in different cases were determined.

Imaging Si NPs and FITC in Cells with FLIM. KB cells were seeded in glass bottom cell culture (Nest Scientific USA) and allowed to adhere for 24 h at 37 °C and 5% CO_2. After removing the medium by 3× washing with PBS, cells were incubated with 50 μg/mL Si NPs or 3 μg/mL FITC in serum-free DMEM at 37 °C and 5% CO_2 for 1.5 h. Afterwards, the cells were washed with PBS and then the cells were covered with PBS in the glass culture dish for imaging experiments.

FLIM data were collected by an avalanche photodiode (PMC-100-1) with a band-pass filter 500±20 nm in the confocal fluorescence microscopy system using XY continuous scanning mode (Olympus FV300, IX71) equipped with a water immersion objective (UplanApo, 60X,1.2 NA), excited by a 405 nm ps laser (BDL-405-SMC) at a repetition rate of 40 MHz. Lifetime maps were calculated on a pixel-by-pixel basis by fitting the lifetime to the intensity decay of each pixel. When we got the various decay time components τ_i of the multi-exponential fitting and the corresponding fractional weights α_i, the intensity-weighted average lifetime ($\bar{\tau}$) in every pixel describing the mean time delay of photon emission after the ps laser pulse was calculated according to Eq (2).

The photobleaching measurements of fluorescence images. KB cells were treated with FITC and Si NPs as described above, respectively. Then the stained cells were

mounted in glass bottom cell culture (Nest Scientific USA). Samples were examined under the laser scanning confocal microscope (LSCM) (Olympus FV300, IX71) with a continuous scanning mode. The cells labeled by FITC were excited by 488 nm laser with 15 mW power. To guarantee fair comparison the Si NPs-labeled cells were excited by 405 nm laser with the same power. The detection windows for FITC and Si NPs are 505−550 nm. The fluorescence images were captured in different time during the continuous laser scanning.

Cytotoxicity assay experiments. 3-(4,5-dimethylthia-zol-2-yl)-2, 5-diphenyltetraz -olium bromide (MTT) was used to measure the cytotoxicity effect of Si NPs on the KB cancer cell line. The cells with the concentration of 3×10^4 cells/mL were seeded in each well of a 96 well flat bottom tissue culture plate and allowed to attach to the plate overnight. The Si NPs were added to the wells with increasing concentrations at 10, 50, 100, 150, 200 μg/mL, respectively. Cells were incubated for 24 h at 37°C. Then, 10 μl MTT solution (5 mg/ml) was then added into each well for incubation of 1.5 h. Finally, the optical densities (O.D) at 450 nm of each well were measured on an iEMS Analyzer (Lab-system). The cell viability in each well was determined by comparing the O.D value with that of untreated control cells in wells of the same plate. All results were presented as the mean ± SE from three independent experiments (n=4 wells each).

pH Stability of Si NPs. The pH effects on emission stability of Si NPs were monitored in 0.1 M phosphate buffer solution, and 0.1 M HCl and 0.1 M NaOH were used to adjust the pH of Si NPs aqueous solution. We measured the fluorescence

intensities of Si NPs at the same concentration of 100 μg/ml in different pH aqueous solutions with a Horiba JobinYvon fluoromax-4 spectrofluorometer.

Acknowledgements

Financial support from the National Natural Science Foundation of China (11074053, 31170802, 20890022 and 21175029) is gratefully acknowledged.

References

1. J. K. Jaiswal, H. Mattoussi, J. M. Mauro and S. M. Simon, *Nature Biotechnol.,* 2003, **21**,47-51.
2. D. R. Larson, W. R. Zipfel, R. M. Williams, S. W. Clark, M. P. Bruchez, F. W. Wise and W. W. Webb, *Science,* 2003, **300**, 1434 -1436.
3. S. Pathak, S. K. Choi, N. Arnheim and M. E. Thompson, *J. Am. Chem. Soc.,* 2001, **123**, 4103-4104.
4. H. Mattoussi, J. M. Mauro, E. R. Goldman, G. P. Anderson, V. C. Sundar, F. V. Mikulec and M. G. Bawendi, *J. Am. Chem. Soc.*, 2000, **122**, 12142–12150.
5. C. A. J. Lin, T. Liedl, R. A. Sperling, M. T. Fernandez-Arguelles, J. M. Costa-Fernandez, R. Pereiro, A. Sanz-Medel, W. H. Chang and W. J. Parak, *J. Mater. Chem.*, 2007, **17**, 1343-1346.
6. A. M. Derfus, W. C. W. Chan and S. N. Bhatia, *Nano Lett.*, 2004, **4**, 11–18.
7. C. Kirchner, T. Liedl, S. Kudera, T. Pellegrino, A. M. Javier, H. E. Gaub, S. Stölzle, N. Fertig and W. J. Parak, *Nano Lett.*, 2005, **5**, 331–338.
8. J. G. C. Veinot, *Chem. Comm.,* 2006, **40**, 4160-4168.
9. J. Zou, R. K. Baldwin, K. A. Pettigrew and S. M. Kauzlarich, *Nano Lett.*, 2004, **4** , 1181–1186.
10. C. Delerue, G. Allan and M. Lannoo, *Phys. Rev. B,* 1993, **48**, 11024-11036.
11. M. Rosso-Vasic, E. Spruijt, Z. Popovic, K. Overgaag, B. van Lagen, B. Grandidier, D. Vanmaekelbergh, D. Dominguez-Gutierrez, L. De Cola and H. Zuilhof, *J. Mater. Chem.*, 2009, **19**, 5926–5933.
12. D. S. English, L. E. Pell, Z. H. Yu, P. F. Barbara and B. A. Korgel, *Nano Lett.*, 2002, **2**, 681-685.
13. J. L. Heinrich, C. L. Curtis, G. M. Credo, K. L. Kavanagh and M. J. Sailor, *Science*, 1992, **255**, 66–68.
14. F. J. Hua, F. Erogbogbo, M. T. Swihart and E. Ruckenstein, *Langmuir*, 2006, **22**, 4363–4370.
15. X. Li, Y. He and M. T. Swihart, *Langmuir*, 2004, **20**, 4720–4727.

16. L. Mangolini, E. Thimsen and U. Kortshagen, *Nano Lett.*, 2005, **5**, 655-659.
17. J. P. and G. A. Samara, *Appl. Phys. Lett.* 1999, 74, 3164-3166.
18. J. D. Holmes, K. J. Ziegler, R. C. Doty, L. E. Pell, K. P. Johnston and B. A. Korgel, *J. Am. Chem. Soc.*, 2001, **123**, 3743–3748.
19. K. A. Pettigrew, Q. Liu, P. P. Power and S. M. Kauzlarich, *Chem. Mater.*, 2003, **15**, 4005–4011.
20. D. Neiner, H. W. Chiu and S. M. Kauzlarich, *J. Am. Chem. Soc.*, 2006, **128**, 11016–11017.
21. M. Rosso-Vasic, E. Spruijt, B. van Lagen, L. De Cola and H. Zuilhof, *Small*, 2008, **4**, 1835.
22. R. D. Tilley, J. H. Warner, K. Yamamoto, I. Matsui and H. Fujimori, *Chem. Commun.*, 2005,**14**, 1833–1835.
23. Z. F. Li and E. Ruckenstein, *Nano Lett.*, 2004, **4**, 1463-1467.
24. S. Sato and M. T. Swihart, *Chem. Mater.,* 2006, **18**, 4083-4088.
25. J. H. Warner, A. Hoshino, K. Yamamoto and R. D. Tilley, *Angew. Chem.,* 2005, **117**, 4626 –4630.
26. Q. Li, Y. He, J. Chang, L. Wang, H. Z. Chen, Y. W. Tan, H. Y. Wang and Z. Z. Shao, *J. Am. Chem. Soc.*, 2013, **135**, 14924–14927.
27. S. X. Li, D. Wei, N. K. Mak, Z. Cai, X. R. Xu, H. B. Li and Y. Jiang, *J. Hazard. Mater.* 2009, **164**, 26-31.
28. D. M. Wassenberg, A. L. Nerlinger, L. P. Battle and R. T. Di Giulio, *Environ. Toxicol. Chem.* 2005, **24**, 2526-2532.
29. Y. L. Zhong, F. Peng, F. Bao, S. Y. Wang, X. Y. Ji, L. Yang, Y. Y. Su, S. T. Lee and Y. He, *J. Am. Chem. Soc.*, 2013, **135**, 8350-8356.
30. Y. He, Y. L. Zhong, F. Peng, X. P. Wei, Y. Y. Su, S. Su, W. Gu, L. S. Liao, S. T. Lee, *Angew. Chem., Int. Ed.*, 2011, **50**, 3080−3083.
31. Y. L. Zhong, F. Peng, X. P. Wei, Y. F. Zhou, J. Wang, X. X. Jiang, Y. Y. Su, S. Su, S. T. Lee, Y. He, *Angew. Chem., Int. Ed.*, 2012, **51**, 8485−8489.
32. Y. Y. Su, F. Peng, Z. Y. Jiang, Y. L. Zhong, Y. M. Lu, X. X. Jiang, Q. Huang, C. H. Fan, S. T. Lee, Y. He, *Biomaterials*, 2011, **32**, 5855−5862.
33. T. Wang, J. Y. Chen, S. Zhen, P. N. Wang, C. C. Wang, W. L. Yang and Q. Peng, *J. Fluoresc.,* 2009, **19**, 615– 621.
34. L. Shang, N. Azadfar, F. Stockmar, W. Send, V. Trouillet, M. Bruns, D. Gerthsen and G. U. Nienhaus, *Small*, 2011, **7**, 2614-2620.
35. M. Jones, J. Nedeljkovic, R. J. Ellingson, A. J. Nozik and G. Rumbles, *J. Phys. Chem. B*, 2003, **107**, 11346-11352.

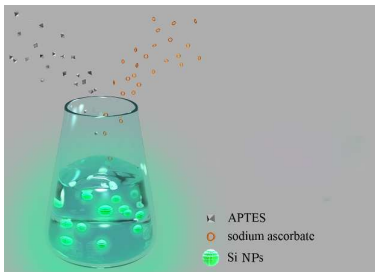

Scheme 1. Schematic illustration of the one-step synthesis of Si NPs.

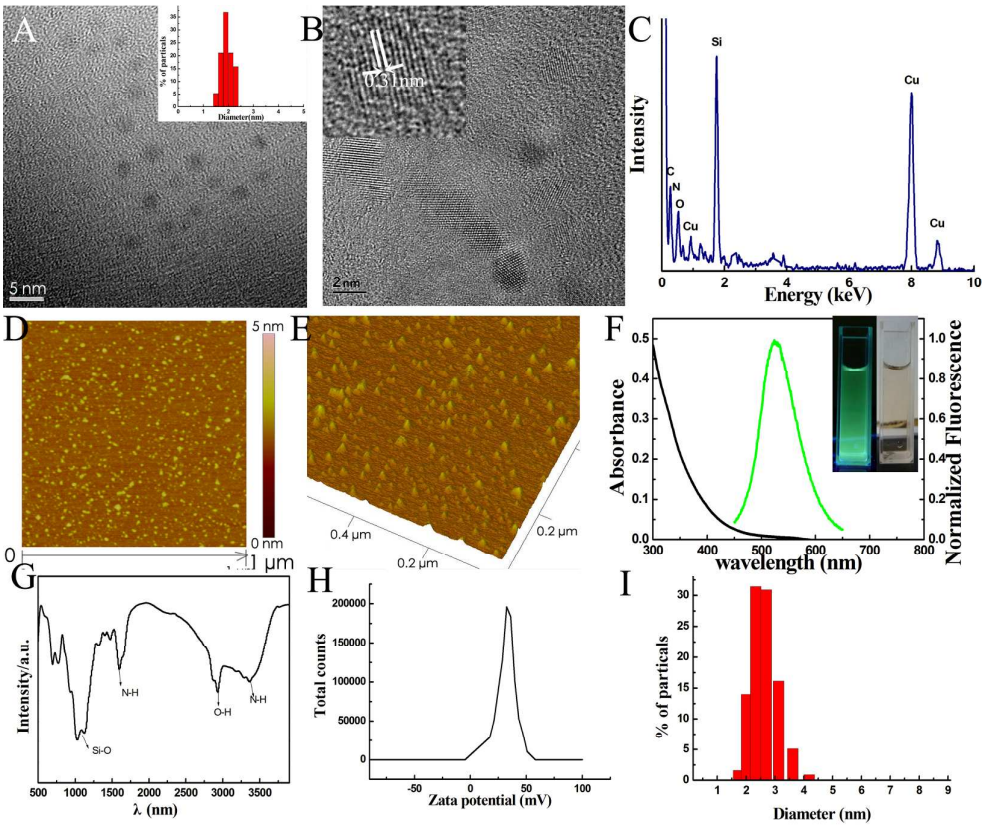

Figure 1. (A) TEM image of the Si NPs. The bar is 5 nm. The inset in (A) presents the diameter distribution of Si NPs measured by TEM. (B) HRTEM images of the Si NPs. A single NP is enlarged in the inset with a spacing of about 0.31 nm. (C) EDS pattern of the Si NPs. (D) AFM image and (E) three-dimensional distribution of the AFM image. (F) The absorbance and emission spectra of Si NPs in aqueous solution. (G) FTIR spectrum of Si NPs. (H) Zeta potential of Si NPs, (I) The diameter distribution of Si NPs measured by DLS.

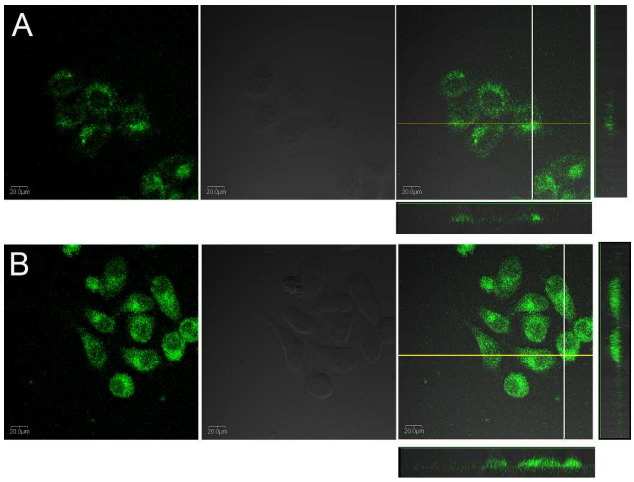

Figure 2. (A) Confocal images of control cells (without any treatments). (B) Distributions of Si NPs in cells. Left: fluorescence images; center: DIC images; and right: merged images. The images displayed below and on the right side of the main image are the x–z and y–z profiles measured by z-scanning along the marked lines in the main images. Scale bar = 20 μm. Excitation: 405 nm laser.

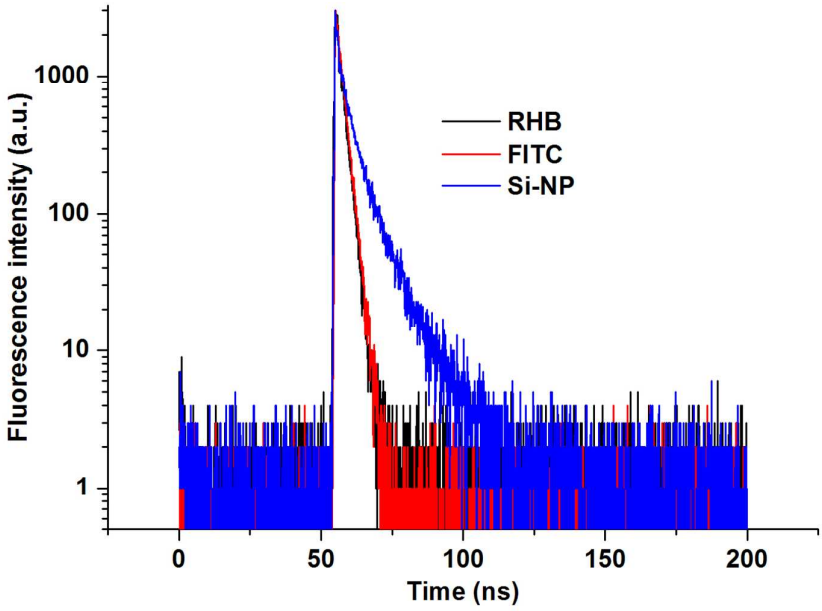

Figure 3. Fluorescence lifetime curves of Si NPs (blue line), FITC (red line) and rhodamine B (RHB) (black line) in aqueous solutions excited by a 405 nm ps laser and measured by TCSPC with a 520±20 nm band-pass filter.

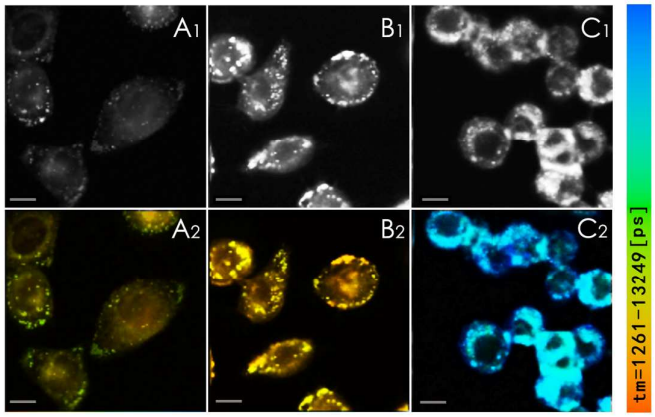

Figure 4. Fluorescence intensity (upper panel) and lifetime (bottom panel) images of KB cells stained with FITC (B), Si NPs (C) and unstained control (A). The fluorescence images were acquired with a 520±20 nm band-pass filter upon excitation of 405 nm ps laser pulse. Scale bar = 20 μm. Colored lifetime bar: 1.2 – 13.2 ns.

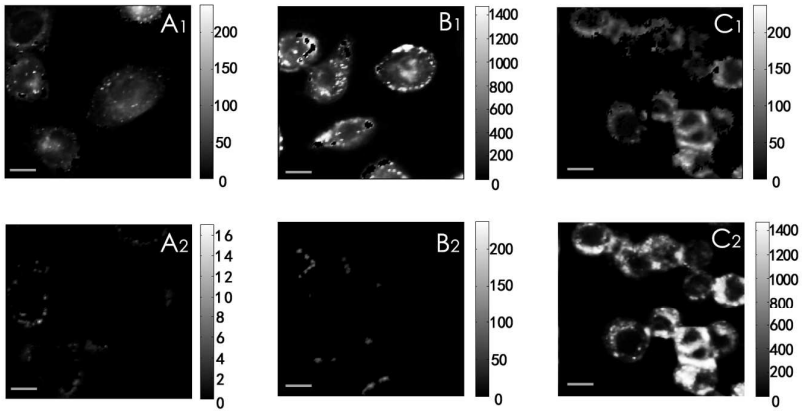

Figure 5. The time-gating fluorescence intensity images of KB cells treated with FITC (B) and Si NPs (C). Control cells are shown in (A). The images in upper row were recorded in time delay of 1-5 ns, and the images in bottom row were acquired in time gating of 5-12 ns after the excitation of the 405 nm ps laser pulse. Scale bar = 20 μm.

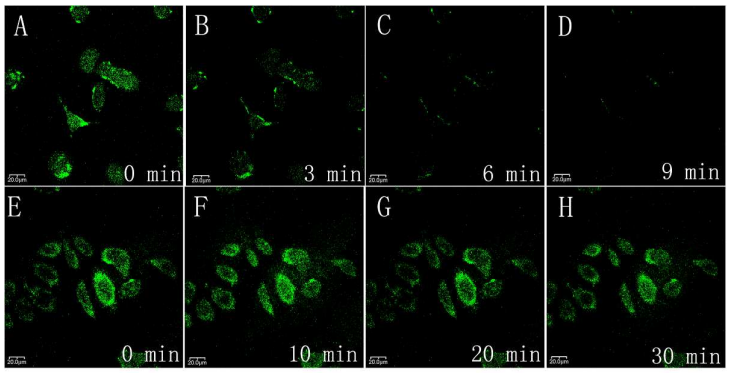

Figure 6. The photobleaching of fluorescence images of cellular Si NPs and FITC under the same power excitation of 405 nm (for Si NPs) and 488 nm (for FITC), respectively, with a continuous laser scanning mode. The upper panel is the fluorescence imaging serial of FITC in KB cells with the scanning time. The bottom panel is for that of Si NPs in KB cells with the scanning time. The excitation power of lasers was 15 mW. The detection window was 505−550 nm.

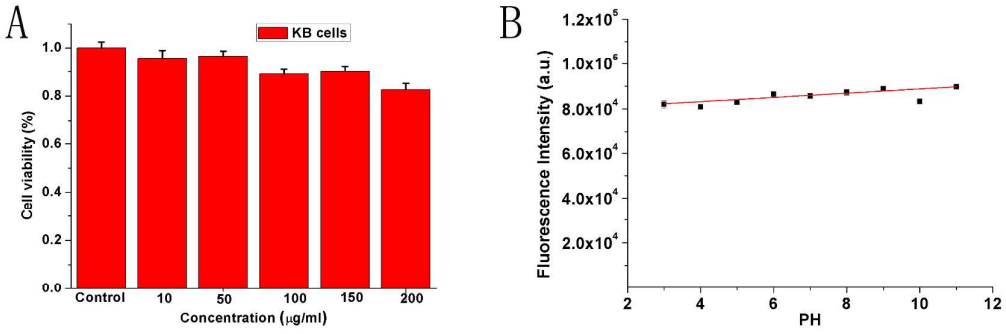

Figure 7. (A) Cell viability (%) measured by MTT assay. The KB cells were incubated with the Si NPs for 24 h at 37°C. All results were presented as the mean ± standard deviation (SD) from three independent experiments with four wells in each. (B) The pH effects on emission stability of the Si NPs in aqueous solution (100 μg/ml).

TOC

Fluorescence intensity (upper panel) and lifetime (bottom panel) images of KB cells stained with FITC (B), Si NPs (C) and unstained control (A).